CONF-900107--2

Corrosion Assessment in FBC Systems*

by

CONF-900107--2

DE90 007806

K. Natesan

Materials and Components Technology Division
Argonne National Laboratory
Argonne, Illinois 60439

January 1990

Invited Paper to be presented at the Fourth Berkeley Conference on "Corrosion–Erosion–Wear of Materials at Elevated Temperatures," January 31 – February 2, 1990, Berkeley, CA.

*Work supported by the U. S. Department of Energy, Office of Fossil Energy, Advanced Research and Technology Development Materials Program, Work Breakdown Structure Element ANL–3, under contract W–31–109–Eng–38.

Corrosion Assessment in FBC Systems*

by

K. Natesan
Materials and Components Technology Division
Argonne National Laboratory
Argonne, Illinois 60439

Abstract

Metallic materials selected for the construction of heat exchangers and tube support structures in fluidized–bed combustion (FBC) systems must withstand the dynamic corrosive conditions prevalent in these systems. Oxidation–sulfidation interactions leading to accelerated metal wastage of components can occur owing to the presence of sorbent deposits on metal surfaces and/or the low–oxygen partial pressures in the exposure environment. A number of laboratory tests were conducted to examine the influence of deposit chemistry, gas chemistry, and alloy pretreatment on corrosion of high–chromium alloys, such as, Incoloy 800 and Type 310 stainless steel. Detailed chemical and physical analyses of spent–bed materials were made and correlated with the observed corrosion behavior of the alloys. A comparative analysis was made of the influence of bubbling–bed and circulating–bed deposits on corrosion of several candidate alloys. Finally, a comparison was made of the laboratory corrosion test data with the metal wastage information developed over the years in several FBC test facilities.

1. Introduction

Combustion of coal in a fluidized bed is widely considered as a viable process for electric power production and for generation of industrial process steam. In power–generating applications, tubes carry a working fluid, either steam or air, which eventually drives a turbine. In steam cycles, the fireside surfaces of superheater tubes operate at temperatures in the range 550–700°C, whereas the temperatures of air tubes can be as high as the bed temperature. In addition, two different types of fluidized–bed combustion (FBC) concepts namely,

Bubbling bed and Circulating fluid bed (CFB) are in vogue today. In the bubbling bed concept, the heat exchanger tubes are immersed in the bed in addition to those in the convective sections of the system, while the heat transfer tubes in a circulating bed are generally situated external to the fluid bed. As a result, the tubes in a CFB are generally exposed to an environment in which coal combustion does not occur (i e., a more stable oxidizing atmosphere will be prevalent) and the tubes will be exposed to a much finer in–bed particles. The system pressure is another important variable in the present concepts. Combustion of coal have been achieved in both atmospheric and pressurized fluid bed combustion (AFBC and PFBC) systems; the method of coal feeding and the sorbent materials used in these systems are different, but the combustion environment prevalent in the two systems is similar. Figure 1 shows schematic diagrams of typical bubbling– and circulating–fluid bed systems.

The temperature at which the fluid beds operate directly affects sulfidation of calcined limestone (CaO) or dolomite (CaO,MgO), NO_x formation from fuel–bound nitrogen, combustion of the coal feed and char recycle, and heat transfer to the in–bed surface. On the basis of these factors, an operating temperature of 900°C has been selected. The design temperature of the in–bed tube materials can range from 500 to 870°C, depending on the system concept and objective. Therefore, the selected alloys for heat exchange should exhibit adequate erosion/corrosion resistance and sufficient mechanical properties at the service temperature. Corrosion and erosion of FBC materials are of practical concern because a number of AFBC and PFBC bubbling units have experienced substantial metal wastage of their in–bed and above–bed components. The components affected have been tube bundles, supports, or feed system units in regular service, or special material probes inserted into the fluidized bed to determine the erosive/corrosive potential in the unit. In some instances, the damage reported appears to have been dominated by erosion; in other instances, evidence of a corrosion or a combined erosion–corrosion type of attack has been detected.

A number of factors, acting singly or in concert with other factors, have been identified as possible causes of metal damage. These factors are as follows: (a) feedstock characteristics such as size, size distribution, hardness, and

chemical composition; (b) mechanical design features such as air distribution geometry, tube bundle geometry, and solids feeder design and location; and (c) operating conditions such as fluidizing velocity, temperature, and gas and solids composition. The environment inside an FBC owing to these factors is complex, and a detailed understanding of the environment as a function of time and position is not fully realized. The environment in an FBC is dynamic and constantly changing, with local regions alternating between oxidizing, reducing, and possibly sulfidizing conditions even though the fluidized bed is operating in an overall oxidizing state. Deposits composed of sulfur sorbent may form on tube surfaces and establish oxidizing–sulfidizing conditions locally underneath the deposit in the vicinity of the deposit/scale interface, thereby accentuate corrosion of materials. In such an environment, many so–called high temperature alloys exhibit inadequate performance owing to the loss of protective adherent oxide scales and subsequent reaction of the base alloy with the gaseous environment, leading to internal oxidation and sulfidation. Numerous research programs have been conducted over the past 15 years to evaluate the performance of materials in FBC environments. Details on the combustion characteristics, coal feedstock and sulfur–sorbent chemistries, operating parameters such as temperature, fluidization velocity, excess air level, and Ca/S ratio are presented in an earlier publications [1,2]. Figure 2 is a representation of how different bubbling–bed systems were operated in terms of two key variables, namely, fluidization velocity and Ca/S ratio.

The purpose of this paper is to review the mechanisms of corrosion in environments characteristic of FBC systems and establish the role(s) of major variables in the corrosion degradation of materials. Laboratory test data and corrosion/erosion information obtained from exposures in large FBC test facilities are used to assess the long–term performance of materials in FBC environments.

2. Material Degradation Mechanisms

Early developers of the FBC process expected that the problems associated with corrosion and erosion of heat exchanger surfaces, as encountered in conventional coal combustion systems, would be minimized by the introduction of fluidized–bed combustion. It was reasoned that the low combustion temperature

would result in considerably less evolution of corrosive species such as alkali salts, and that the buildup and subsequent sintering of deposits on heat exchangers would be less than in conventional systems, thus deterring fireside corrosion. In practice, traditional fireside corrosion featuring attack by molten salt species has not been reported in FBCs; however, a form of oxidation–sulfidation has been observed.

The environment experienced by materials exposed in a fluidized–bed atmosphere is both mechanically and chemically hostile to metals, and the concern over the corrosion/erosion potential for in–bed metal parts has resulted in a number of test programs identified in Fig. 2. In addition, a number of laboratory studies have been conducted in which selected alloys, coatings, and weldments were exposed to simulated FBC environments with and without the sulfur–sorbent deposits. The corrosion and erosion data obtained from all these studies have shown a considerable variation in the extent of degradation among specimens exposed in different locations within the same bed as well as among specimens exposed in different beds of nominally similar environments. To rationalize this varying behavior of materials in FBC systems, attempts have been and are being made to understand the chemical and physical nature of the in–bed environment and its effect on materials.

2.1. Characterization of the in–bed environment

In recent years, efforts have been made in a number of programs to measure oxygen partial pressure in the FBC environment in situ, using solid electrolyte cells. The results showed significant variations in the cell response with both axial and radial positions in the bed, thereby indicating that the oxygen concentration in the bed was not uniform but varied in the range 10^{-3} to 10^{-14} atm. Further, the cell measurements indicated that the oxygen pressure in any given location within the bed fluctuated between high and low values with an oscillation period of less than one second. In contrast to the direct measurement of oxygen pressure in the bed of an FBC, the sulfur pressure in the gas phase is determined largely by the thermodynamic equilibrium between CaO and sulfated lime ($CaSO_4$), both of which are present in significant quantity during the bed operation. The sulfur pressure in the gas phase obtained by this method may be quite different from that present under the deposit at the deposit/scale interface.

Figure 3 shows the CaO–CaS–$CaSO_4$ phase stability fields calculated for temperatures of 704, 840, and 900°C. Superimposed on this plot is the oxygen–sulfur dashed curve calculated using thermodynamic equilibria between various gas species in the combustion environment at 900°C. Since $CaSO_4$ and CaO are always present in the bed, the partial pressures of oxygen and sulfur in the bed will follow along the CaO–$CaSO_4$ equilibrium line. On this basis, the lowest value of oxygen pressure that can be attained is ~2×10^{-12} atm at 900°C and the corresponding sulfur pressure is ~10^{-6} atm.

2.2. Effect of gas environment in the bed

The fluidized–bed combustion of coal produces gas that contains principally O_2, CO_2, H_2O, SO_2, and N_2, with minor amounts of SO_3, nitrogen oxides, chlorides, and other volatilized salts. The composition of the gas depends importantly on the air/coal stoichiometric ratio. In addition, the SO_2 concentration in the gas phase will be determined by the type and amount of sulfur sorbent and the sulfur content of the coal used in the combustion process. Figure 4 shows the calculated thermochemical diagrams for iron, chromium, and nickel at 566 and 840°C, indicating the thermodynamic stability of various oxide and sulfide phases [3]. From these diagrams and the oxygen partial pressures measured in various FBC systems, it is evident that $CaSO_4$ should be the thermodynamically stable phase in the deposit. The extent of interaction between the deposit and the substrate or the deposit and the scale depends on three factors: the porosity of the deposit layer and the transport of gaseous molecules containing sulfur, the dissociation of $CaSO_4$ to establish a sulfur pressure at the underside of the deposit, and the rate of reaction between the underlying alloy elements and the reactants such as oxygen and sulfur to form oxide/sulfide scales and internal penetration of oxygen/sulfur into the substrate.

At metal temperatures below 600°C, where alloys such as carbon steel and low chromium–molybdenum steels are used, the alloys predominantly develop external scales that consist of iron oxide and and the internal layers of either iron sulfide or a mixture of iron sulfide and chromium sulfide. As the SO_2 reacts to form oxides of the substrate elements, the released sulfur reacts to form iron sulfide which also acts as a fast diffusion path for additional penetration of sulfur.

In alloys with intermediate chromium levels (e.g., Fe–9Cr–1Mo steel), an internal layer of chromium oxide and/or chromium sulfide forms. At higher chromium levels, e.g., alloys such as 310 stainless steel and Alloy 800, the scales consist of thin chromium–rich oxides, but the scale thicknesses and depth of sulfur penetration increase with an increase in metal temperature. The oxide scales are porous in nature, however, and they generally contain a sulfide phase that results from the reaction between the base metal constituents and the sulfur released from the reaction of Cr or Al (in Cr_2O_3–forming or Al_2O_3–forming alloys, respectively) with SO_2. The porosity of the scale enables gas SO_2 molecules to permeate to the scale/substrate interface and cause internal sulfidation. In the laboratory studies[3] a decrease in the oxygen (and corresponding increase in sulfur) partial pressure in the exposure environment, even in the absence of deposits, can lead to an increase in corrosion scale thickness and depth of internal penetration for a number of alloys of interest in FBC application. Further, metal wastage (i.e., scale thickness and internal penetration) is much more pronounced as the exposure temperature or time increases. In addition, alloys exposed to substoichiometric combustion environments exhibited iron and/or nickel sulfide corrosion product layers. In general, the high–nickel alloys exhibited severe attack in comparison with the iron–base alloys. Figure 5 shows the effect of the combustion stoichiometric condition on the depth of corrosive penetration in Incoloy 800 and Types 310 and 347 stainless steel that were tested for 250 hr at several bed temperatures[4]. For a given in–bed test condition, an increase in metal exposure temperature leads to only a small increase in scale thickness, but the depth of internal penetration in the substrate material can increase significantly. Even though the gas environment alone can have an effect on the corrosion behavior of materials, the components in FBC systems will always be covered by a deposit of bed material; as a result, an understanding of the corrosion behavior of materials in the presence of a combination of deposit and the gas atmosphere is essential and will be discussed in the next section.

2.3. Effects of deposits and gas chemistry

The deposits in FBC systems are typically a mixture of CaO, $CaSO_4$ (also Mg compounds in the case of PFBCs), ash constituents, and carbon particles. The manner in which these constituents are deposited on the metallic surfaces is

not well established; however, a typical deposit has been reported to consist of particles less than 1 μm in diameter with densities of the deposit >99%. However, such high densities could have resulted from chemical reactions that can occur within the deposit and physical sintering of deposit constituents over long periods of time at elevated temperatures in the bed.

Deposit Only

Laboratory studies[3] have shown that (a) $CaSO_4$ deposit alone can initiate sulfidation in iron– and nickel–base alloys at temperatures of 593°C and higher and (b) sulfidation of the alloys does not require the presence of sulfur in the gas phase. These experiments, conducted with $CaSO_4$–coated low–chromium ferritic steel specimens in an argon environment, indicated the following: (a) a significant outward transport of iron occured from the substrate material into the $CaSO_4$ deposit, and no such migration of chromium occured; (b) the reaction product at the deposit/alloy substrate interface consisted of two distinct layers, an outer layer of predominantly iron oxide and an inner layer of iron sulfide and chromium–rich oxides; and (c) chromium–rich sulfides precipitated at the grain boundary region of the substrate alloy. In contrast with the results on ferritic steels, there was virtually no migration of iron from the alloy substrate into the deposit in the high–chromium alloys such as Type 310 stainless steel and Incoloy 800. The oxide scales that developed in these alloys were predominantly Cr–rich oxide or $CaCr_2O_4$. The sulfur that is released during the oxidation reaction penetrated the substrate alloy and precipitated Cr–rich sulfides at the grain boundary regions. Figure 6 shows the scale thickness and intergranular penetration data for the $CaSO_4$–coated alloys exposed to the argon environment at different temperatures.

Variation in Synthetic Deposit Chemistry

Experiments were also conducted to examine the combined sorbent/gas chemistry effect on the corrosion of structural alloys over a wide range of metal temperatures, different gas chemistries, gas cycling conditions, and different types of deposits[3,5]. Figure 7 shows scanning electron microscopy (SEM) photographs of corrosion product layers that developed on Incoloy 800 specimens coated with deposit mixtures 1 through 4 (identified as lines for 1 through 3 and a

point for 4 in the p_{O_2}-p_{S_2} diagram in Fig. 7) after exposure at 840°C to a gas mixture with oxygen and sulfur partial pressures of 5.4×10^{-12} and 1.6×10^{-8} atm, respectively. The four synthetic deposit mixtures will lead to oxygen and sulfur partial pressures dictated by the following chemical reactions:

$$CaO + 1/2\ S_2 = CaS + 1/2\ O_2 \qquad \text{Mix 1}$$

$$CaS + 2\ O_2 = CaSO_4 \qquad \text{Mix 2}$$

$$CaO + 1/2\ S_2 + 3/2\ O_2 = CaSO_4 \qquad \text{Mix 3}$$

$$CaO + CaS + 1/2\ S_2 + 7/2\ O_2 = 2\ CaSO_4 \qquad \text{Mix 4.}$$

Specimens coated with mixtures 1, 2, and 4 exhibited sulfidation attack in these experiments whereas the specimen coated with mixture 3 still developed a thin Cr-oxide scale. The implication of these tests is that, in the presence of mixtures 2 and 4 and SO_2 in the gas phase, a fairly high p_{S_2} and low p_{O_2} can be established in the pores of the deposit material and in the deposit/alloy interface region. Consequently, the alloy has a tendency to undergo sulfidation attack in these two tests. In the presence of mixture 1 and SO_2 in the gas phase, the dominant reaction in the deposit will be sulfation of CaO, which will result in an increase in p_{O_2} and p_{S_2} in the pores of the deposit; however, the p_{O_2} will still be below that dictated by the CaO/CaS/$CaSO_4$ triple point. As a result, the alloy will undergo sulfidation attack and Ni sulfide and Fe oxide will be the reaction product phases. In the presence of mixture 3 and SO_2 in the gas phase, the dominant reaction in the deposit will be sulfation of CaO to $CaSO_4$ which can decrease the p_{S_2} in the pores of the deposit material and the alloy will have a tendency to undergo oxidation. On the other hand similar experiments conducted with Type 310 stainless steel showed (see Fig. 8) only oxidation mode of attack in the presence of any of the four deposit mixtures. However, these specimens were only exposed for ~100 hr at elevated temperature. It has been shown earlier[5] in 3000hr tests, that the presence of $CaSO_4$ deposit and a low p_{O_2}/moderate p_{S_2} gas mixture can trigger sulfidation of the underlying base alloy even in Type 310 stainless steel, but the extent of attack is much less than that in Incoloy 800.

Pretreatment of the Specimens

The role of two different pretreatments (namely, preoxidation and precarburization) of alloy specimens in the subsequent corrosion of the alloys in the presence of different deposit mixtures and gas environments was examined. In the preoxidation treatment, the alloys were oxidized for ~80 hr at 840°C in sulfur-free gas atmosphere with a p_{O_2} of 3.6×10^{-14} atm. In the precarburization treatment, the specimens were carburized at 840°C in a 5 vol.% CH_4-H_2 gas mixture for 64 hr.

Figure 9 shows the SEM photographs of the morphologies of initially preoxidized Incoloy 800 specimens coated with deposit mixtures 1 through 4 and exposed at 840°C to a gas mixture with oxygen and sulfur partial pressures of 5.4×10^{-12} and 1.6×10^{-8} atm, respectively. Preoxidation of the specimens in a low-p_{O_2} environment produced thin Cr-rich oxide scales on the specimens. Subsequent exposure of the specimens to the deposit mixtures in the presence of a SO_2-containing gas mixture had no deleterious effect on the preformed oxide scales indicating that sulfidation of Cr_2O_3 scale (once developed) is extremely slow and is not of concern from the standpoint of corrosion.

In the precarburization treatment, the gas mixture (namely, 5 vol.% CH_4-H_2) established a carbon activity of unity; and carburization of the alloy specimens in such an environment simulates carbon pick up in the alloy due to the deposition of unburnt carbon (i.e., incomplete combustion of coal or in the vicinity of coal feed ports) on the alloy components. The precarburization for ~64 hr at 840°C resulted in extensive precipitation of (Cr,Fe) carbides in the alloy. As a result, the effective Cr concentration and activity in the alloy decreased and caused the alloy to behave (from scaling standpoint) as a medium-Cr alloy. For example, if carburization proceeds via the reaction,

$$23/6\ Cr(\gamma) + C(\gamma) = 1/6\ Cr_{23}C_6 \text{ (in mixed carbide)},$$

where $Cr(\gamma)$ and $C(\gamma)$ are concentrations of Cr and C in the austenite phase, the free-energy change for the reaction, as a function of temperature ($\Delta F^\circ = -16380 - 1.54\ T$), and the equilibrium constant for the reaction,

$$K = a^{1/6}_{Cr_{23}C_6} / a_{C(\gamma)} a^{23/6}_{Cr(c)},$$

can be used to calculate the Cr activity/concentration in the austenite phase for a given level of carbide precipitation. At a carbon activity of ~0.3, up to which $M_{23}C_6$ carbide is stable, the precipitation of carbides can lower the Cr content in the matrix phase to less than 15 wt.%. At carbon activities above 0.3, M_7C_3 and M_3C carbides will precipitate and further decrease the Cr activity in the austenite phase.

Figure 10 shows SEM photographs of initially carburized Incoloy 800 specimens that were coated with deposit mixtures 1 through 4 and exposed at 840°C to a gas mixture with oxygen and sulfur partial pressures of 5.4×10^{-12} and 1.6×10^{-8} atm, respectively. Exposure of the precarburized specimens leads to the formation of nonprotective surface scales in the presence of all the deposit mixtures investigated. A comparison of photographs in Figs. 7 and 10 shows that precarburization has little effect on the morphology of the scale layers and that the layers are somewhat thicker in the precarburized specimens. Sulfidation is the mode of attack in this alloy either with or without precarburization treatment. Figure 11 shows the SEM photographs of scale layers that developed on Type 310 stainless steel after exposure to oxygen-sulfur environments in the presence of different deposit mixtures. The photographs show a substantial amount of carbide precipitation but the thicknesses of scale layers are much smaller than in Incoloy 800, confirming a superior corrosion resistance of the Type 310 stainless steel even with carburization pretreatment. These results also indicate that carburization is not an essential precursor to subsequent sulfidation, and the alloy scaling behavior of the carburized alloys is determined by the effective chromium concentration in the austenite matrix.

3.0. Effect of Spent-bed Materials

Spent-bed materials were obtained from four different test facilities such as TVA 20MW, IEA/Grimethorpe, Nova Scotia/Point Tupper, and CE/Lurgi fluidized beds. Among these, the first three were bubbling–bed type while the fourth was a circulating–bed type. In addition, the IEA/Grimethorpe facility is a pressurized unit whereas the others are atmospheric combustors. Spent–bed

materials from the TVA facility were obtained at two different time periods, during which either Reed or Fredonia limestones was used as a sulfur sorbent.

3.1. Characteristics of spent-bed materials

The bed materials were sieved through several U.S. Standard sieves of successfully smaller apertures, each sieve being shaken for ~10 min to allow smaller particles to fall through to the next sieve. The sieving separated the powders into different particle–size ranges, which were weighed and recorded as weight–percent of the total amount of material. Figure 12 shows the weight–percent of the material collected in the sieves for four different spent–bed materials.

Figure 13 shows the particle–size distribution for the four spent–bed materials used. The distribution indicates that ~40 wt.% of the material is of particle size ~1690 μm and is essentially the same for the three different FBC materials. The Fredonia limestone is much softer than the Reed limestone, and this difference is reflected in a much larger amount of finer size particles in the run with the Fredonia limestone. Table 1 lists the chemical compositions of spent–bed materials obtained from different systems. Analysis was conducted for two different size fractions, namely, –8+18 and –40+60 mesh sizes (average particle sizes of ~1690 and 335 μm, respectively) to examine chemical differences, if any, between different size fractions. Several inferences can be made from the results presented in Table 1: (a) the K_2SO_4 content is much larger in the TVA–bed material than from others and the concentration is approximately the same in the runs with Fredonia and Reed limestones, indicating that it is probably coal–related rather than that due to sulfur sorbent; (b) the CFB ash has a very low amount of alkali sulfate when compared with those from bubbling–beds; (c) the $CaSO_4$ content of the bed material was also extremely low in the CFB ash when compared with those of bubbling beds; (d) a wide variation in SiO_2 and Al_2O_3 content is observed in the materials from different bubbling beds; (e) the calculated values for the free silica (probably quartz) in the materials range between 0.5 to 38.0 wt.%, if one assumes that all the alumina in the spent–bed material is present as dehydrated Kaolinite (with a composition of $Al_2O_3.2SiO_2$). The highest value was obtained for the Grimethorpe material with an average

particle size of ~1690 μm; (f) the calculated value for the free silica amount in the CFB ash is ~27.6 wt.%. In general, the particle size of the material (in the vicinity of heat recovery system) in CFB units is much smaller than in the bubbling–bed units.

3.2. Effect of bubbling-bed deposits

The in-bed environment in bubbling-bed combustion systems, in general, has p_{O_2} values in the range from 10^{-2} to 10^{-3} atm; however, fluctuations in p_{O_2} values to as low as 10^{-14} have been measured with an oxygen sensor. The time interval for fluctuations in the p_{O_2} values has been less than a second. Under these conditions, the heat exchanger materials and support structures will be exposed to an alternating high p_{O_2}/low p_{O_2} atmosphere with a cycle time of a second or less. In order to evaluate the effect of spent-bed materials on the corrosion of candidate materials, three different gas environments (identified as A, B, and C in Figure 14) were selected. Gas mixture A has p_{O_2} and p_{S_2} values of 7×10^{-3} and 2.6×10^{-28} atm, respectively, which typify the flue-gas environment. Gas mixture B has p_{O_2} and p_{S_2} values of 5.4×10^{-12} and 1.6×10^{-8} atm, respectively, which represent the reducing environment during gas cycling. Gas C has a p_{O_2} value of 3.6×10^{-14} atm and has no sulfur, representing a reducing atmosphere without sulfur. It has been shown earlier, that sustained exposure (500 to 2000 hr) of structural materials to gas mixture B in the presence of $CaSO_4$ or $CaSO_4$/CaO deposit can lead to internal sulfidation in the alloys[3,5]. As a result, gas mixtures A and C were used along with the spent-bed materials from different FBCs to evaluate corrosion susceptibility of candidate materials.

Figure 15 shows SEM photographs of scale layers that developed on Incoloy 800 and Type 310 stainless steel specimens coated with a reagent grade $CaSO_4$/CaO mixture and spent-bed materials from the TVA AFBC and Grimethorpe PFBC facilities. The top row of photographs shows the morphologies that developed when Incoloy 800 specimens with the deposits were exposed to gas mixture A (typical of flue-gas atmosphere). The specimens developed thin Cr-oxide scales in the presence of all three deposits. The middle row of photographs shows morphologies of scales that developed when the specimens with the deposits were exposed to gas mixture C, a low-p_{O_2}

atmosphere without sulfur. It is evident that the scales are predominantly Fe and (Fe,Cr) oxide and (Fe,Ni) sulfide, and consequently, nonprotective in nature. The thicknesses of the scale layers ranged from 0.30 to 1.2 mm; the thicker layers in the presence of spent-bed materials are indicative of the more aggressive nature of the bed material to Incoloy 800 compared with that of the reagent grade material. Further, the source of S for sulfidation of these specimens is the deposit materials since the gas phase included no S-containing species. Also, in the absence of deposit (i.e., source of S), Incoloy 800 specimens would have developed thin Cr-oxide scales when exposed to the low-p_{O_2} atmosphere that was used in these tests. The bottom row of photographs shows the morphologies of scales that developed when Type 310 stainless steel specimens with the deposits were exposed to the sulfur–free low p_{O_2} atmosphere. The scales were thin and composed of oxide and sulfide phases with some intergranular precipitation of sulfides in the substrate alloy. The results conclusively indicate that composition of the deposit material, the local gas phase environment, and alloy chemistry must be considered in an evaluation of oxidation–sulfidation behavior of candidate heat exchanger materials for FBC applications.

3.3. Corrosion in bubbling–bed vs. in CFB environments

Extensive testing of materials have been conducted to develop corrosion information on a variety of ASME–coded and noncoded structural alloys, coatings, and weldments under well–characterized laboratory environments that simulate both bubbling– and CFB atmospheres[5]. In these experiments, ring specimens were used to simulate the heat exchanger tubes exposed to an environment arising from the combustion of coal. In addition, a number of experimental alloys were exposed in the form of flat coupons to evaluate their corrosion resistance. The outer surfaces of the ring specimens and one surface of the flat coupons were coated with either reagent–grade $CaSO_4$ (simulating bubbling–bed deposit) or CFB ash. The specimens were exposed for a total time period of 3000 hr at a metal temperature of 871°C while the gas phase was maintained at ~900°C. The corrosion test probes were cooled to room temperature after every 500 hr of exposure at the test temperature. During the cooldown period, the specimens were recoated with the deposit material to ensure that there was no starvation of reactant for the continuation of the corrosion process.

Gas mixture B (see Fig. 14) and compressed air were used to simulate the bubbling–bed and CFB conditions,respectively.

During the course of this study, the deposit materials were collected from the corrosion probes after every 500 hr intervals and analyzed. Table 2 lists the composition of the deposits for various time periods for both the bubbling-bed and CFB simulations. In the bubbling-bed case, initially pure reagent grade $CaSO_4$ decomposed as a function of time and after 500 hr of exposure, the deposit had 51.2 wt.% CaO and only 7.9 wt.% $CaSO_4$. Since gas B (with lower p_{O_2} and higher p_{S_2} than flue gas atmosphere) was used in this simulation, the dissociation of $CaSO_4$ is favored within the deposit; and the sulfur released via the dissociation reaction led to sulfidation of the substrate alloy. No Cr_2O_3 phase was detected in the deposit material. As the exposure time increased beyond ~1000 hr, the extent of $CaSO_4$ dissociation became less and the process is probably controlled by the transport of sulfur and oxygen through the already formed scale. In the case of CFB simulation, the initial composition of the ash changes very little with exposure time. During the initial ~500 hr, the deposit contained Cr_2O_3 and some additional Fe_2O_3 indicative of oxide scaling in this simulation. These results indicate that the deposit chemistry is influenced both by the gas chemistry in the exposure environment and the scaling kinetics at the alloy/deposit interface. Consequently, the local oxygen and sulfur partial pressures within the deposit can be widely different and can change with time, at least in the early periods of exposure.

Figure 16 shows the corrosion–product morphologies observed on the deposit side of Types 304 and 310 stainless steel and Incoloy 800 specimens after 3000–hr exposures in the two test environments. The figure shows that Type 304 stainless steel with a chromium content of ~18 wt.% predominantly developed (Cr,Fe) oxide scales in the presence of either deposit. The scale thicknesses were fairly small, and the substrate exhibited a significant amount of carbide precipitation at the grain boundaries. $CaSO_4$–coated Type 310 stainless steel, even though it contained 25 wt.% Cr, developed a ragged oxide scale with substantial internal penetration of sulfur. On the other hand, CFB–ash coated Type 310 stainless steel developed Cr oxide scale and virtually no sulfur was detected either in the scale or the substrate alloy. In general, Type 310 stainless

steel was susceptible to the formation of (Fe,Cr) sigma phase during thermal exposure. An Incoloy 800 specimen coated with reagent grade $CaSO_4$ underwent severe sulfidation indicating susceptibility of a higher nickel (32.5 wt.%) containing alloy to sulfur attack. On the other hand, the same alloy coated with CFB ash developed a (Cr,Fe) oxide scale (with no trace of sulfur) indicating that negligible sulfur pressure established via dissociation of sulfur containing ash components in the deposit layer. Similar corrosion information has been developed for a number of alloys exposed to simulated FBC environments[5]. Table 3 is a summary of data on scale thickness, depth of penetration, and metal recession for several alloys exposed for 3000 hr at temperatures between 871 and 900°C in simulated bubbling–bed and CFB environments. The contrasting corrosion behavior of several alloys in the presence of $CaSO_4$ and CFB ash deposits indicates that the sulfur partial pressure established by the $CaSO_4$ deposit and low–p_{O_2} gas environment (simulating a bubbling bed) is much higher than that present in CFB ash/air atmosphere (simulating a CFB).

4.0 In-Bed Materials Data

From the preceeding section materials (especially high–chromium alloys exposed to an FBC environmen) can undergo oxidation-sulfidation corrosion and that life expectancy of components would be strongly influenced by the internal sulfidation penetration of the substrate materials. Furthermore, the bed chemistry in terms of oxygen and sulfur partial pressures is not uniform; therefore, different tubes in a heat exchanger, although made of the same alloy, could be exposed to widely differing and varying (oxidizing to reducing) conditions in the bed. A viable alloy must exhibit acceptable corrosion rates even under the most extreme reducing conditions ($p_{O_2} = 10^{-12}$ to 10^{-14} atm) in the bed. In general, metallic heat–exchanger tubes are coated with a dense and sometimes thick deposit, the composition of which is dependent on gas chemistry, exposure time and temperature. The in–bed wastage data, developed over the years, in general, indicate that the erosion contribution will not be significant for components that operate at temperatures between 650 and 900°C; however, since the erosion processes in FBCs are not well understood, and a few instances of unanticipated catastrophic erosion of in–bed cooling tubes have been reported. Thus, the interpretation of metal wastage data calls for caution. These

difficulties not withstanding, the materials data base has been reviewed earlier [1,2] to evaluate the time and temperature dependence of the wastage, scale thickness plus internal penetration, and corrosion rates for several alloys or classes of alloys tested in FBC systems. The data for a few of the alloys are summarized below.

Figure 17 is a plot of the scale thickness alone and scale thickness plus penetration depth versus in–bed exposure time for Type 310 stainless steel at temperatures between 810 and 871°C in several FBC systems. The data indicate that the scale thickness is negligibly small and increases to a constant value after 2000 hr of exposure. The depth of penetration is approximately three times that of scale thickness and probably has an increasing trend with exposure time. One may infer from the data that the alloy has not undergone "breakaway" corrosion during the time period of exposure. In addition, the 10,000–hr data from the Nova Scotia test facility show that the alloy has an acceptable corrosion behavior.

Figure 18 is a plot of corrosion rate for Type 310 stainless steel versus in–bed exposure temperature obtained over a wide range of conditions and exposure times in several FBC test facilities. Corrosion rate calculations were made on the assumption of parabolic kinetics (i.e., the amount of degradation proportional to the square root of the duration of exposure) for both scale thickness and penetration depth. In some instances where scale thickness and penetration data are not reported, the metal loss information was used to calculate corrosion rates. A comparison of the laboratory– and in–bed data shows that the former is higher by a factor of two; however, the laboratory data were obtained in a much more reducing environment (i.e., oxygen and sulfur partial pressures in the vicinity of the CaO–CaS–$CaSO_4$ triple point) and can be considered as an upper bound rate for the material from the standpoint of corrosion.

Figure 19 is a plot of scale thickness and depth of penetration for Incoloy 800 versus exposure time in various FBC systems. It is evident from this figure that, although the scale thickness is fairly insensitive to exposure time beyond ~2000 hr, the penetration depth increases dramatically, especially in the 10,000–hr exposure results of Nova Scotia Power. Figure 20 shows the corrosion rate, based on parabolic kinetics, as a function of alloy exposure temperature. Over the entire

temperature range, the corrosion rate is approximately twice that observed for Type 310 stainless steel. Further, the long–time performance of the alloy is not promising, since the life–limiting parameter, namely, the internal penetration depth, increases significantly with exposure time. In addition the alloy is susceptible to catastrophic oxidation–sulfidation corrosion when exposed to low–p_{O_2} environments, as evidenced by the laboratory test results discussed in earlier sections of this paper.

The information presented in this paper establishes the role of several key variables in corrosion of candidate structural materials for FBC application and also aids in understanding the mechanism of corrosion in the dynamic environment of the FBC system. At present, the results are not sufficient to establish the design parameters and operating guidelines that will result in a long, reliable, economical life for FBC components. Materials degradation depends on local conditions that are prevalent in the vicinity of the area of attack, and these can fluctuate significantly over small intervals of distance and time The establishment of quantitative relationships among operating parameters and process condition measurements (as independent, controllable variables), and local bed conditions in the vicinity of in–bed component materials and the corrosion/erosion behavior of those components (as dependent variables) would be a significant step up in FBC technology development.

5.0. Summary

One major materials issue in the commercialization of FBC systems is the corrosion degradation of heat–exchange components and the uncertainty in life assessment. This paper addressed the role of several key variables such as deposit chemistry, gas chemistry, and alloy pretreatment in the oxidation–sulfidation behavior of candidate structural alloys. Several deposit mixtures involving combinations of reagent grade CaO, CaS, and $CaSO_4$, and spent–bed materials from TVA 20MW, IEA/Grimethorpe, Nova Scotia, and CE/Lurgi CFB facilities were used in the study to evaluate the effect of deposit chemistry on the corrosion process.

The laboratory test results established the gas chemistry and deposit compositions that can lead to accelerated oxidation–sulfidation corrosion of

materials. The results also showed that the scale thickness and internal penetration in the presence of CFB ash were much less than those obtained with $CaSO_4$ or spent–bed materials from bubbling–bed units. From the corrosion standpoint, a number of commercial/engineering alloys can be expected to perform in an acceptable manner over a long period of time in CFB units, primarily due to the fact that the sulfur pressure established by the CFB ash is negligible. Based on the test results, a similar conclusion cannot be reached for materials performance in bubbling–bed systems. A comparison of laboratory test data, developed in a low–p_{O_2} environment, with the in–bed corrosion data showed that the rates are higher by a factor of ~2 in the laboratory tests and these rates can be treated as an upper bound value, if the alloys are not susceptible to breakaway corrosion.

Acknowledgments

This work was supported by the U. S. Department of Energy, Office of Fossil Energy, Advanced Research and Technology Development Materials Program, Work Breakdown Structure Element ANL–3, under contract W–31–Eng–109–38. D. L. Rink assisted with the experimental program and the microstructural analyses of exposed specimens.

References

1. K. Natesan, S. A. Miller, and W. F. Podolski, An assessment of the performance of heat exchanger materials in fluidized bed combustors, Argonne National Laboratory Report, ANL–86–42, February 1987.
2. K. Natesan, S. A. Miller, and W. F. Podolski, Performance of materials in fluidized–bed combustors, J. Mater. Engg., 9 (1987) 269.
3. K. Natesan, Role of FBC deposits in the corrosion of heat exchanger materials, High Temp. Technol., 4 (1986) 193.
4. A. J. Minchener, P. T. Sutcliffe, I. S. Scott, R. S. Courtney, D. M. Lloyd, D. C. Read, T. Golesworthy, and J. E. Oakey, Materials evaluation for fluidized–bed combustion systems, Report CS–3511, Electric Power Research Institute, Palo Alto, CA (1984).
5. K. Natesan and W. F. Podolski, Laboratory Tests in Support of Atmospheric Fluidized–Bed Cogeneration Air Heater Experiment: Summary Report, Argonne National Laboratory Report, ANL-88–36, July 1988.

Table 1. Composition (in wt.%) of Spent–Bed Material from Different FBCs

Component	Nova Scotia		TVA (Fredonia)		TVA (Reed)		Grimethorpe		CFB ash
	–8+18	-40+60	-8+18	-40+60	-8+18	-40+60	-8+18	-40+60	
SiO_2	29.5	28.4	6.1	2.4	11.3	5.5	42.6	14.3	51.4
Al_2O_3	14.4	10.5	1.9	1.6	1.5	1.1	3.9	1.7	20.2
Fe_2O_3	3.2	4.8	2.5	2.6	1.3	1.4	4.6	2.5	9.1
$CaSO_4$	35.5	39.0	51.5	56.0	52.2	62.4	34.4	58.6	6.5*
K_2SO_4	11.5	12.1	31.2	33.3	26.3	22.4	9.1	15.4	5.4
Na_2O	0.08	0.07	0.06	0.06	0.09	0.09	0.08	0.08	0.1
MgO	0.9	1.0	1.5	0.8	1.7	0.9	1.0	0.7	1.1
TiO_2	–	–	–	–	–	–	–	–	0.8
LOI+	5.0	4.1	5.1	3.2	5.5	6.2	4.2	6.7	3.1

* Mixture of CaO and $CaSO_4$

+ Loss on ignition

Table 2. Variation in the chemical composition of deposit as a function of exposure time

Deposit in Bubbling–Bed Simulation

Deposit Component	Exposure Time (hr)						
	0	500	1000	1500	2000	2500	3000
$CaSO_4$	99.2	7.9	5.1	–	71.7	63.7	69.2
CaO	0	51.2	57.8	–	21.7	22.8	26.0
SiO_2	0	3.8	–	–	2.4	1.4	1.9
Al_2O_3	0	0.3	–	–	0.2	0.2	0.1
Fe_2O_3	0	0.5	–	–	2.1	1.4	2.0
LOI*	–	35.5	23.7	–	1.9	10.4	0.7

Deposit in CFB Simulation

Deposit Component	Exposure Time (hr)						
	0	500	1000	1500	2000	2500	3000
$CaSO_4$	–	12.4	8.8	10.0	10.6	8.7	10.5
CaO	9.2	2.2	4.4	4.0	3.6	5.0	4.0
SiO_2	51.4	37.0	40.8	43.2	43.4	44.0	43.8
Al_2O_3	20.2	17.2	35.9	32.8	31.7	31.1	31.5
Fe_2O_3	9.1	11.9	8.4	6.8	6.9	8.0	7.1
Cr_2O_3	0	16.7	2.3	–	–	–	–
LOI*	3.1	0.5	0.5	0.6	0.6	0.5	0.5

*Loss on ignition

Table 3. Scale thickness, depth of penetration, and metal recession data for several alloys exposed for 3000 hr in simulated FBC environments

Material	With $CaSO_4$		With CFB Ash		Metal Recession	
	Scale Thickness Average (μm)	Penetration Depth Average (μm)	Scale Thickness Average (μm)	Penetration Depth Average (μm)	With $CaSO_4$ (μm)	With CFB Ash (μm)
304	20	23	24	14	65	134
800	Destroyed		27	30	-	128
RA 330	70	150	NE	-	193	NE
310	70	230	17	62	250	160
316	10	40	NE	-	98	NE
188	Internal attack		NE	-	-	NE
347	NE	-	32	40	NE	210
253 MA	30	65	33	18	105	70
HK40	Destroyed		NE	-	-	NE
FW-4C	5	100	NE	-	203	NE
HR-3C	20	65	NE	-	125	NE
Mn-Nb-mod. 800H	Destroyed		NE	-	-	NE
430	NE	-	120	48	NE	340
54E	30	33	33	15	80	60
53C	10	16	30	30	50	84
RV 8413	15	4	15	18	15	45
IC-50	Destroyed		50	30	-	80
FA-41	10	7	15	18	15	30
IC-266*	Destroyed		18	72	-	90

* - Preoxidized sample.
NE - Not exposed.

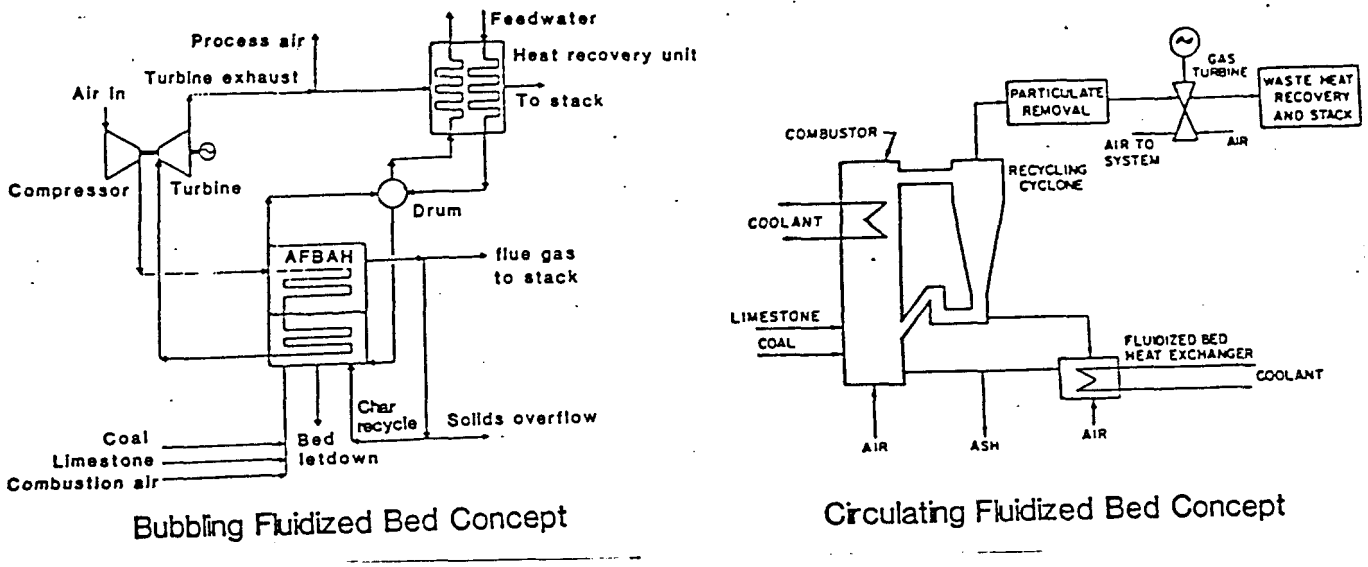

Figure 1. Schematic diagrams of bubbling– and circulating–bed systems.

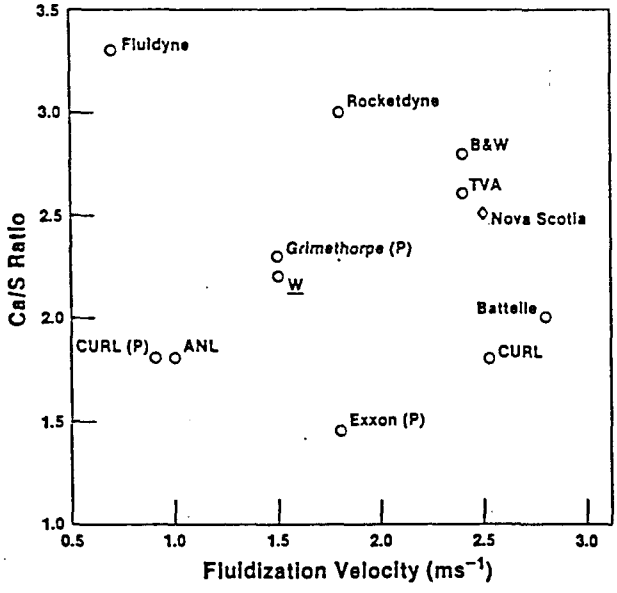

Figure 2. Fluidization velocity and Ca/S ratio combinations for the materials tests conducted in various bubbling FBC systems. P in parentheses signifies pressurized unit; all others are atmospheric units.

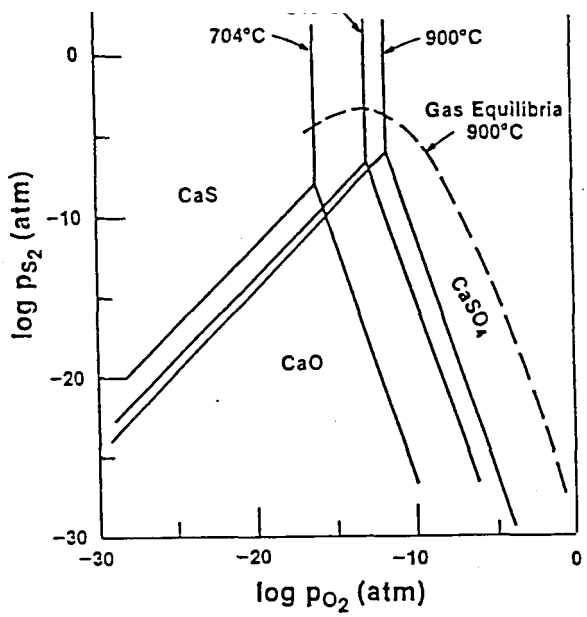

Figure 3. $CaO–CaS–CaSO_4$ phase-stability fields calculated for several temperatures. The dashed line represents thermodynamic gas phase equilibria in the combustion atmosphere.

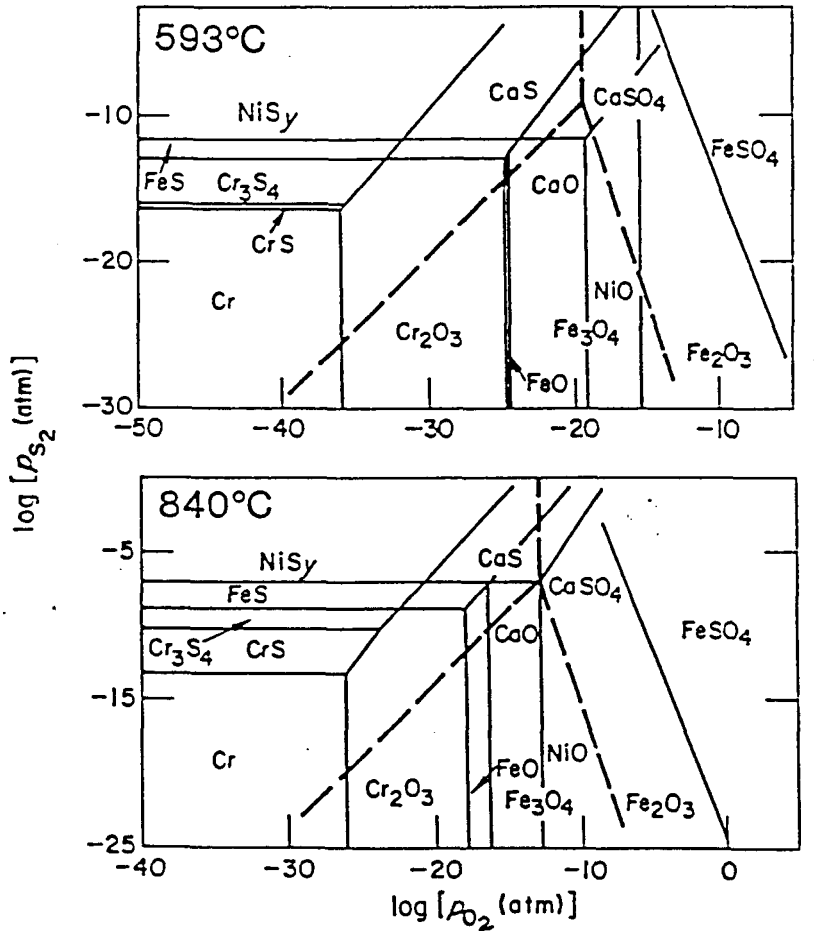

Figure 4. Oxygen–sulfur thermochemical diagrams at 566 and 840°C, depicting regions of stability of various oxide and sulfide phases. The phase fields for the $CaO–CaS–CaSO_4$ system (dashed lines) are also shown.

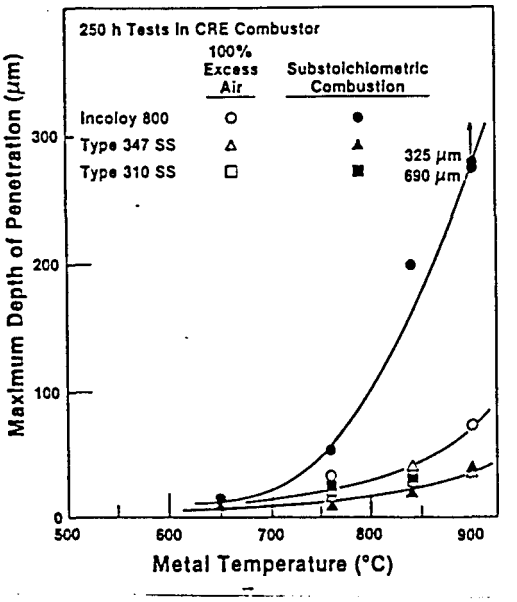

Figure 5. Effect of combustion stoichiometry on corrosion of in–bed alloys.

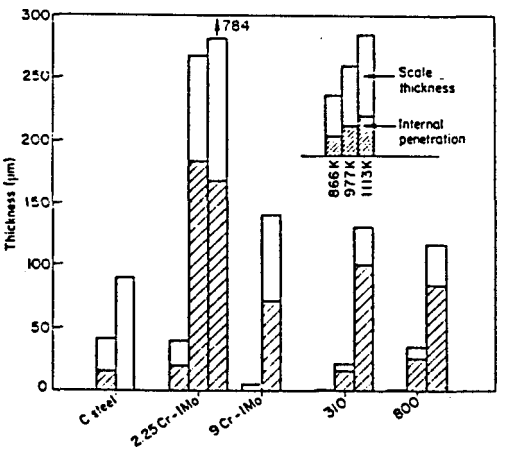

Figure 6. Scale thickness and intergranular penetration data for $CaSO_4$–coated alloys after 500 hr exposures to a flowing argon environment.

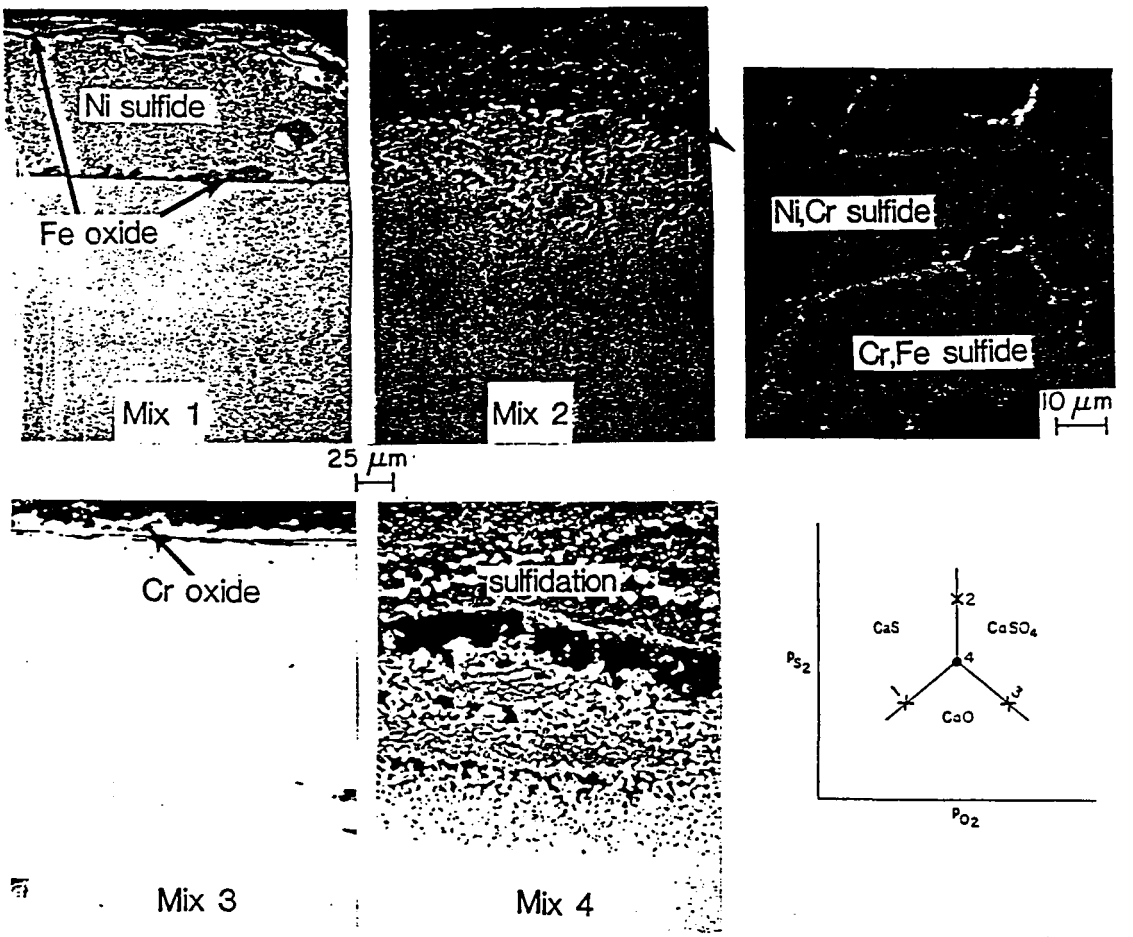

Figure 7. Morphologies of scale layers developed on Incoloy 800 specimens coated with different deposit mixtures and exposed to a gas mixture with oxygen and sulfur partial pressures of 5.4×10^{-12} and 1.6×10^{-8} atm, respectively.

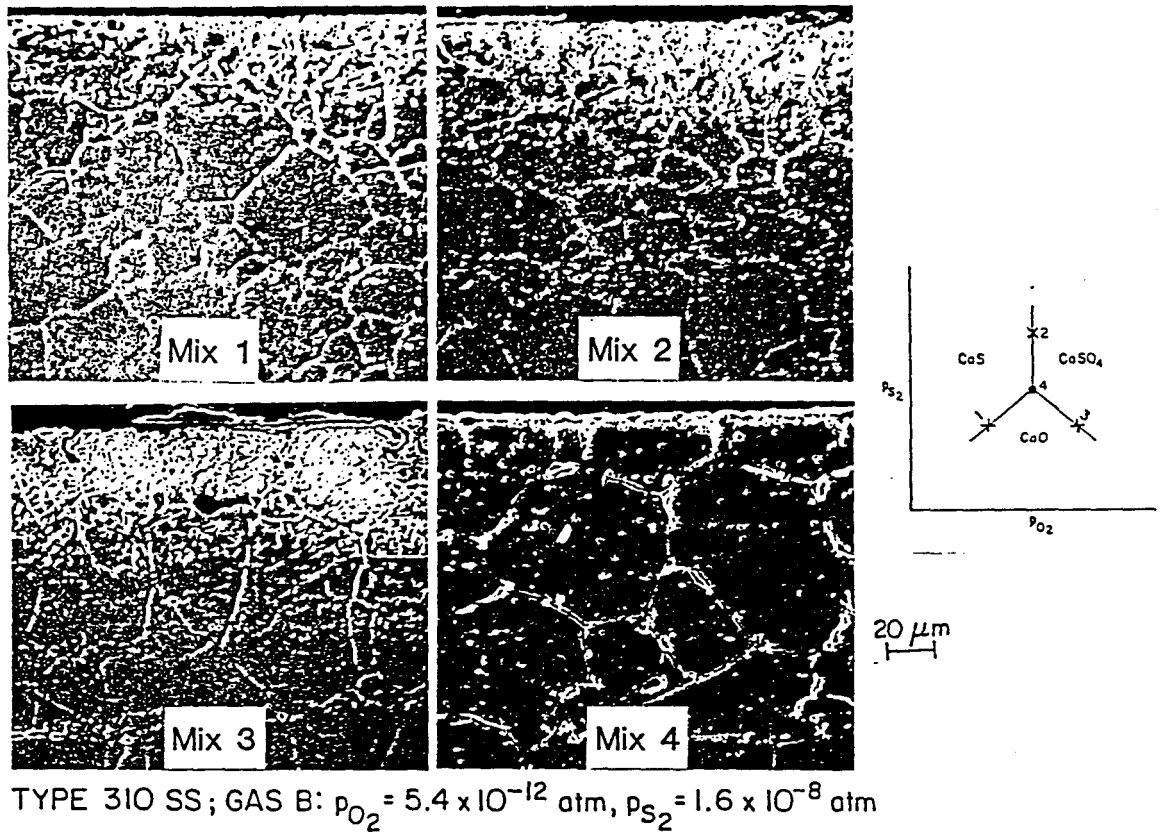

Figure 8. Morphologies of scale layers developed on Type 310 stainless steel specimens coated with different deposit mixtures and exposed to a gas mixture with oxygen and sulfur partial pressures of 5.4×10^{-12} and 1.6×10^{-8} atm, respectively.

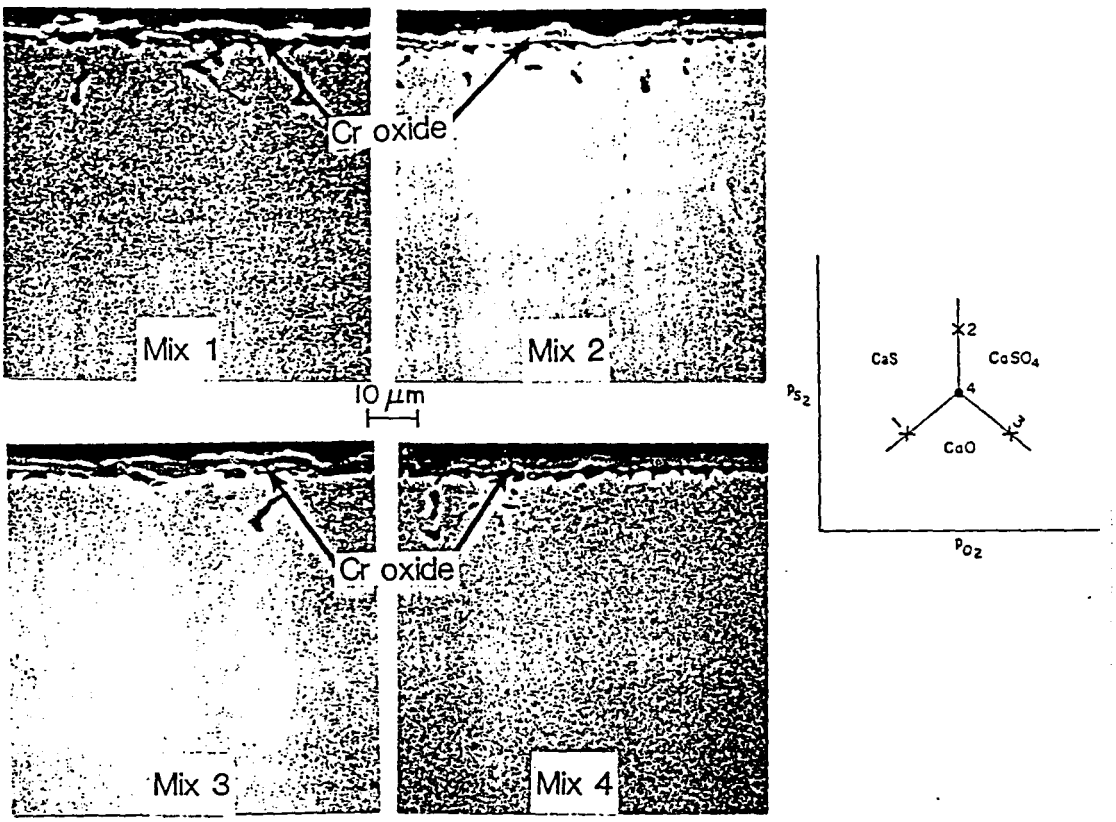

Figure 9. Morphologies of scale layers developed on initially oxidized Incoloy 800 specimens that were coated with different deposit mixtures and exposed to a gas mixture with oxygen and sulfur partial pressures of 5.4×10^{-12} and 1.6×10^{-8} atm, respectively.

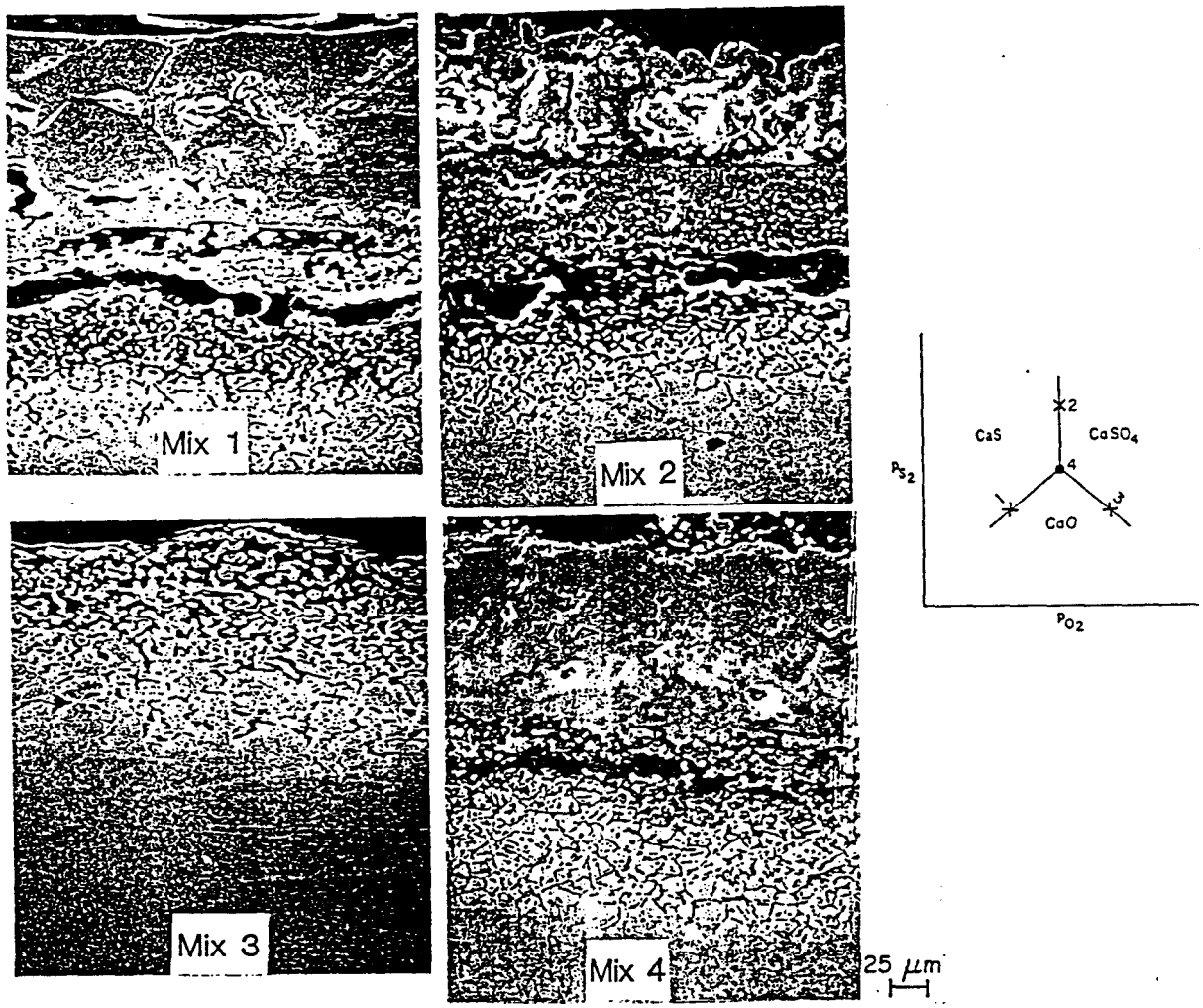

Figure 10. Morphologies of scale layers developed on initially carburized Incoloy 800 specimens that were coated with different deposit mixtures and exposed to a gas mixture with oxygen and sulfur partial pressures of 5.4×10^{-12} and 1.6×10^{-8} atm, respectively.

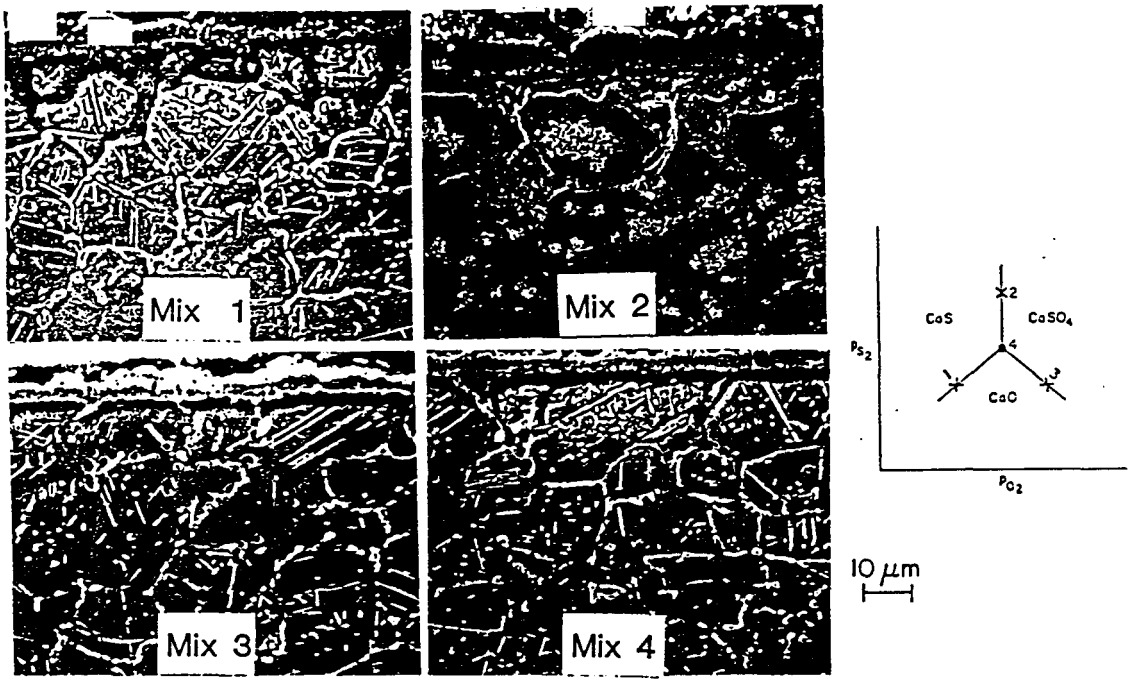

Figure 11. Morphologies of scale layers developed on initially carburized Type 310 stainless steel specimens that were coated with different deposit mixtures and exposed to a gas mixture with oxygen and sulfur partial pressures of 5.4 x 10^{-12} and 1.6 x 10^{-8} atm, respectively.

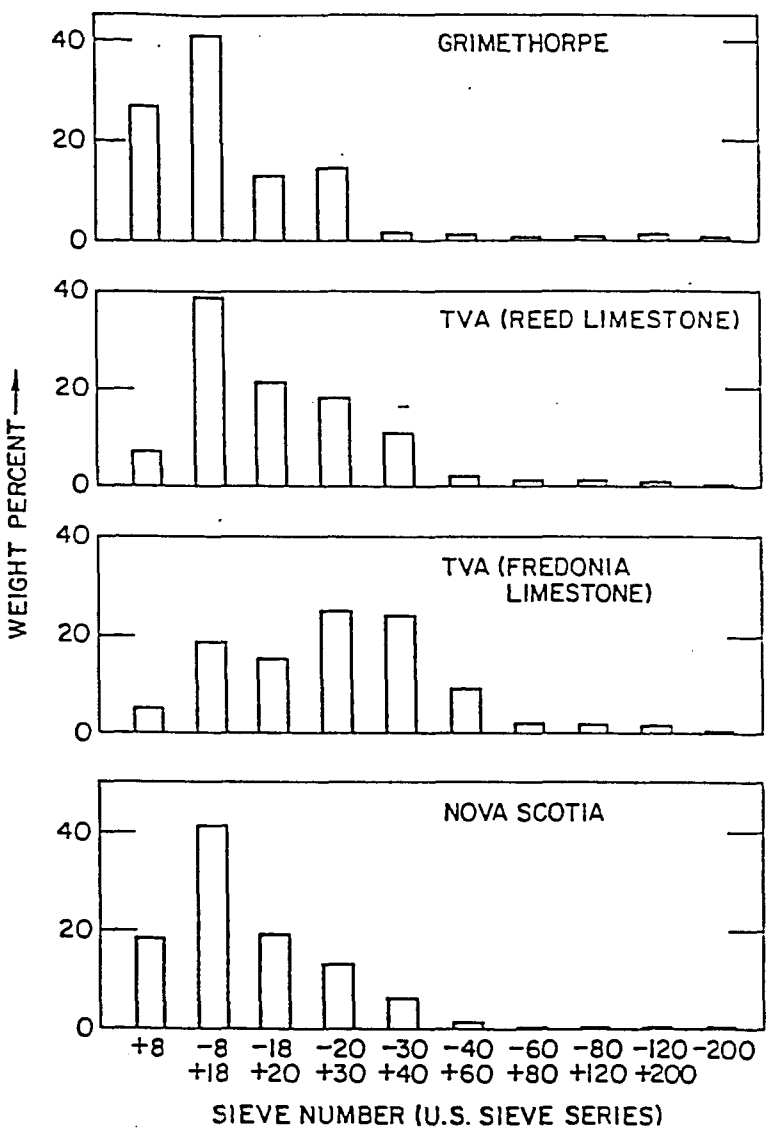

Figure 12. Weight distribution of spent–bed materials obtained from different FBC systems.

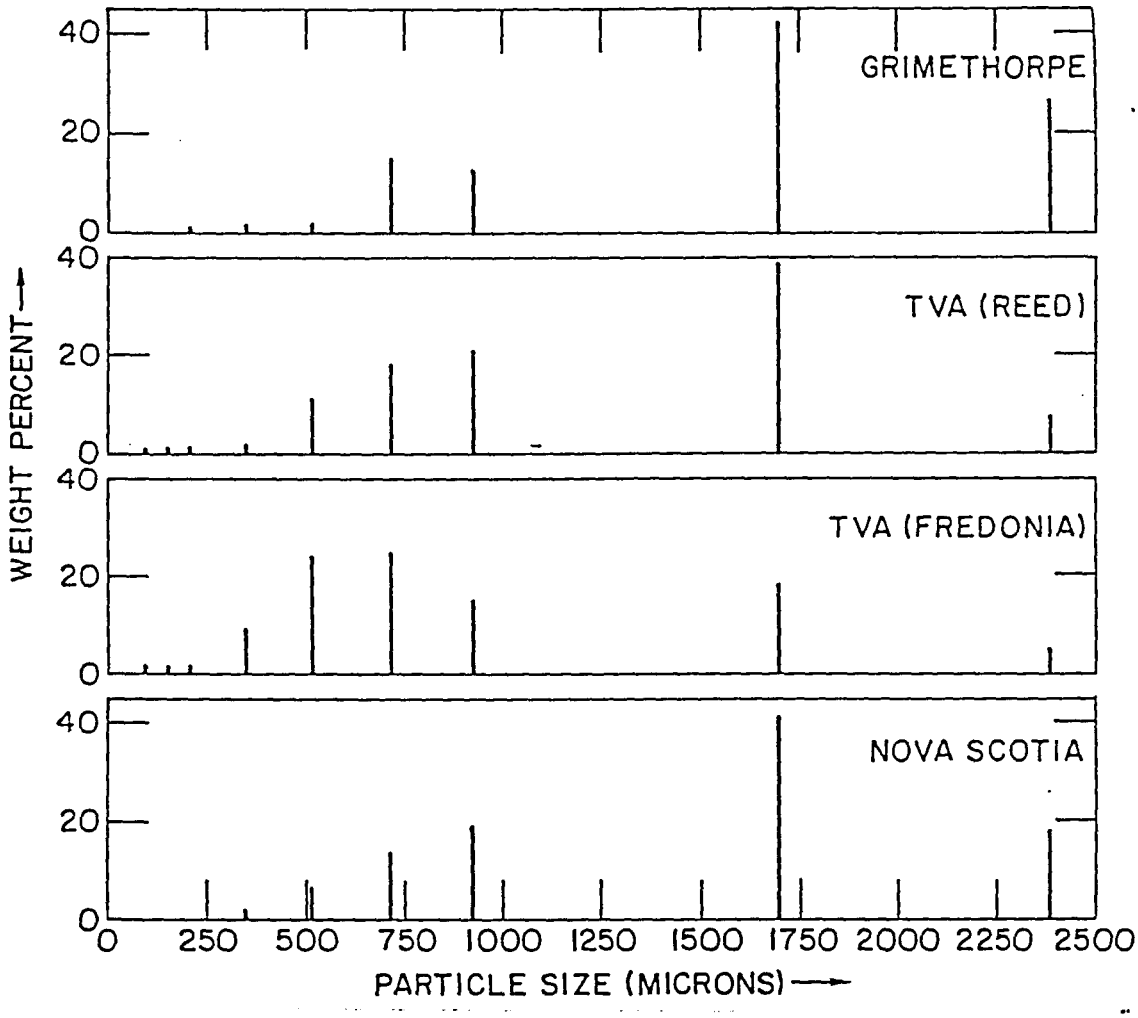

Figure 13. Particle–size distribution for the spent–bed materials obtained from different FBC systems.

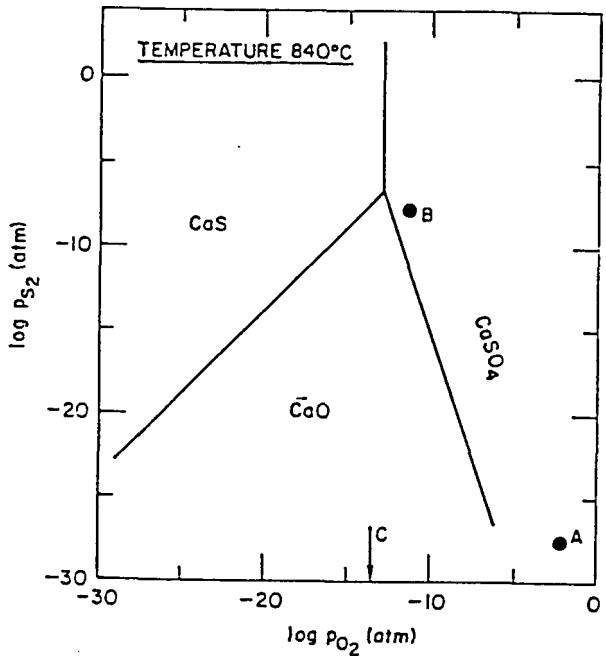

Figure 14 Ca-S-O stability diagram indicating the gas environments A, B, and C used in the experiments with deposit materials from different FBC facilities.

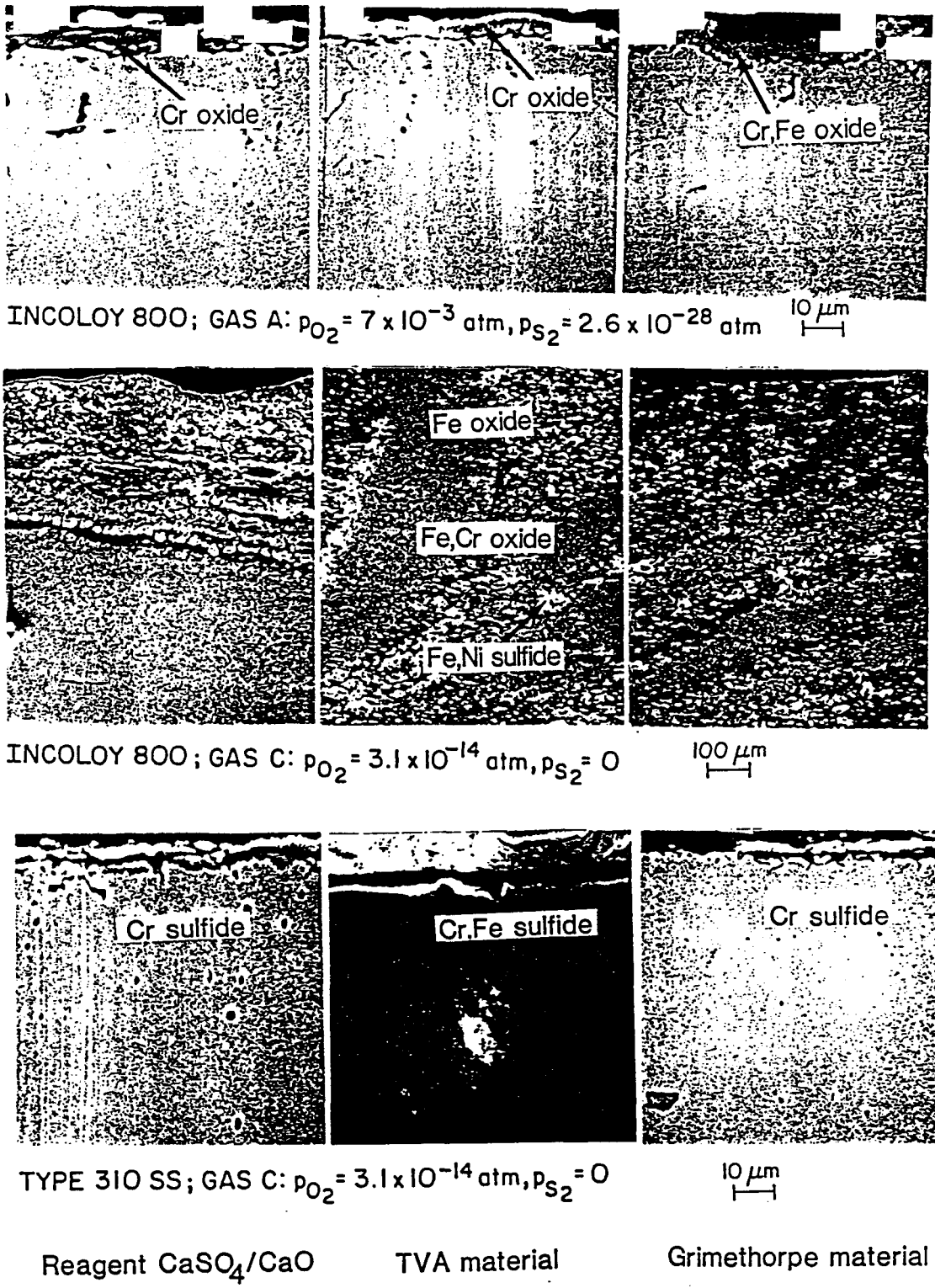

Figure 15. Corrosion scale morphologies developed on Incoloy 800 and Type 310 stainless steel coated with reagent grade CaO-$CaSO_4$ mixture and spent-bed materials from TVA and Grimethorpe and exposed to different gas mixtures.

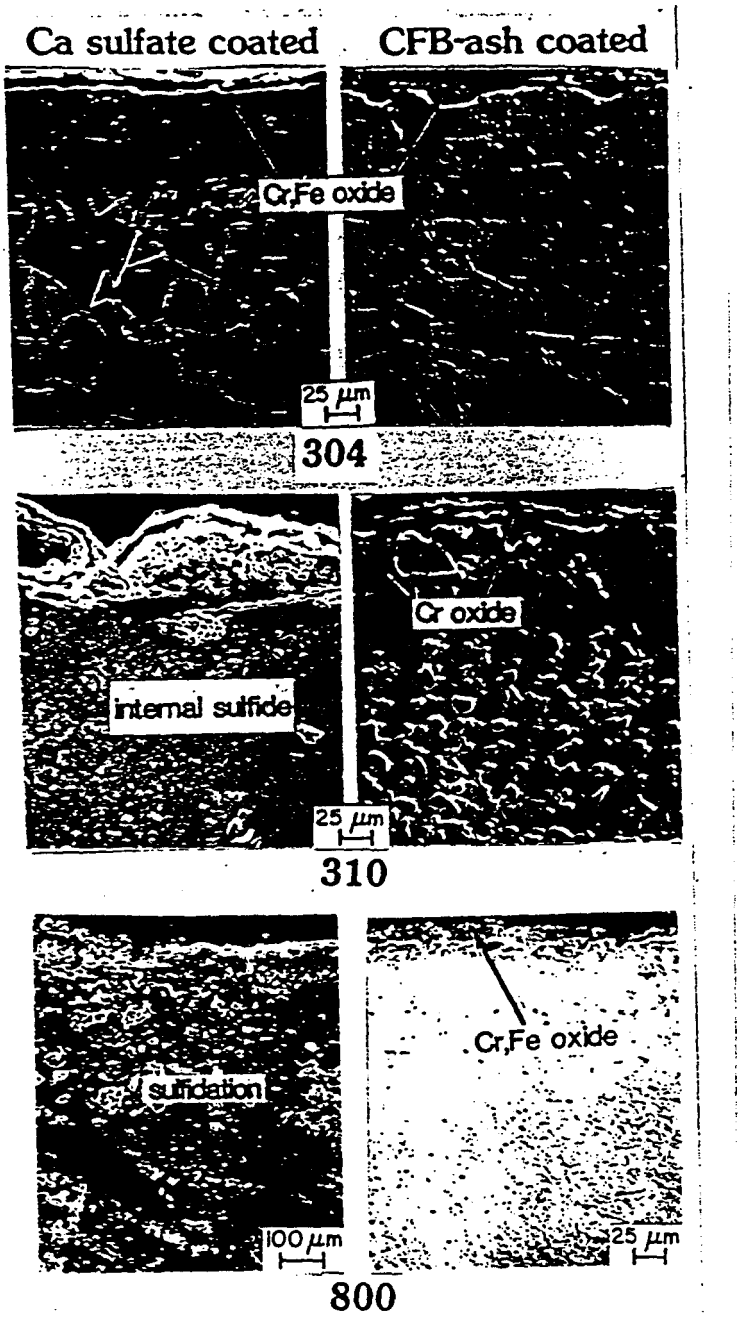

Figure 16. Microstructures of specimens of Types 304 and 310 stainless steel and Incoloy 800 with either $CaSO_4$ or CFB ash deposit after 3000–hr exposure at 871°C.

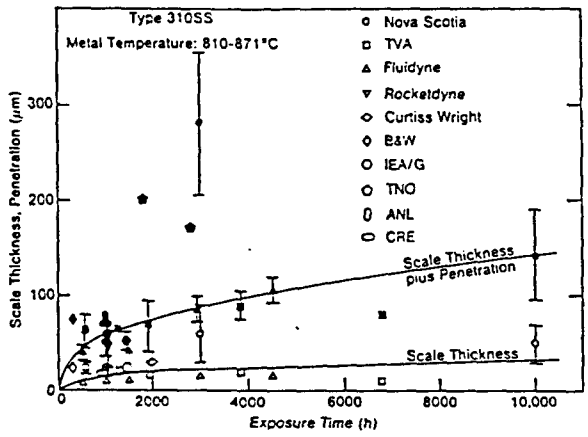

Figure 17. Scale thickness and penetration depth data for Type 310 stainless steel.

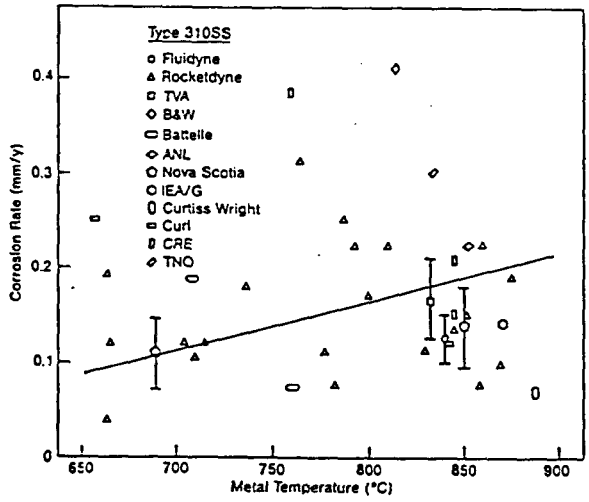

Figure 18. Corrosion rate variation with temperature for Type 310 stainless steel.

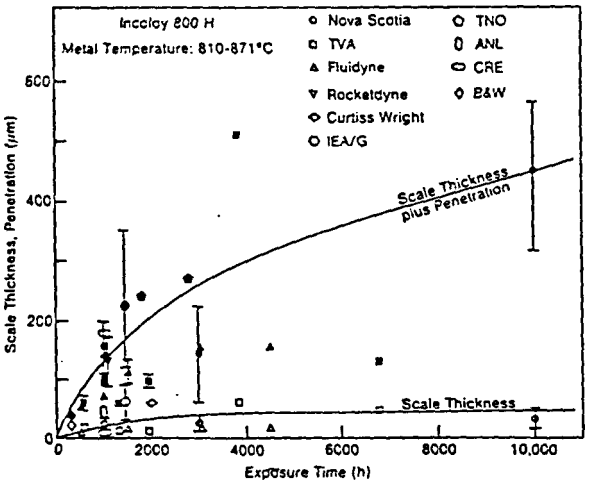

Figure 19. Scale thickness and penetration depth data for Incoloy 800.

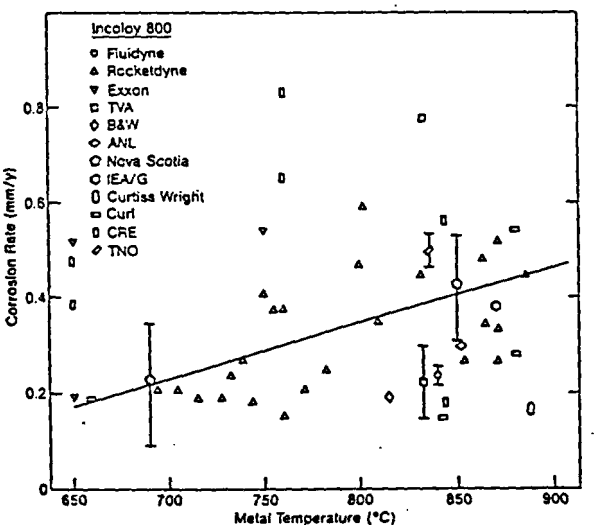

Figure 20. Corrosion rate variation with temperature for Incoloy 800.